Journal of Solid State Chemistry **166,** 197–202 (2002)
doi:10.1006/jssc.2002.9582, available online at http://www.idealibrary.com on IDEAL®

Laser Ablation Deposition of CeO_{2-x} Epitaxial Domains on Glass

W. H. Lee and P. Shen[1]

Institute of Materials Science and Engineering, National Sun Yat-sen University, Kaohsiung, Taiwan, Republic of China

Received December 4, 2001; in revised form February 28, 2002; accepted March 8, 2002

Laser ablation of CeO_2 target in vacuum (5×10^{-4} Pa) was used to produce nanometer-size condensates, which deposited as yellowish top coating and whitish bottom coating on a soda-lime glass substrate. The top coating consists of optically anisotropic columnar domains conformable to monoclinic Ce_6O_{11} phase coexisting with cubic (*c*) CeO_{2-x}, whereas the bottom coating is optically isotropic *c*-CeO_{2-x} due to oxygen uptake from the substrate. Transmission electron microscopy indicated that the columnar domains are made up of defective fluorite-type nanoparticles, which tended to coalesce over (111) plane to form dislocations and (111)-preferred orientation, an artificial epitaxy owing to rotation–coalescence of {111} faceted CeO_{2-x} condensates on the amorphous substrate and/or within the coating.

Key Words: **CeO_{2-x} condensate; glass substrate; laser ablation deposition; artificial epitaxy.**

1. INTRODUCTION

CeO_2 was widely used as a support of metals for catalytic oxidation reactions (1, 2). In general, the catalytic activity of oxides is derived through their provision of adsorbed surface oxygen species for reactions, and/or easy extraction of their lattice oxygen to form oxygen vacancies in the oxide structure. CeO_2 film also fits silicon-on-insulator structures, stable capacitors for ultralarge-scale integration (ULSI) and buffer layers of superconducting materials because of its chemical stability, high dielectric constant ($\varepsilon_r \sim 26$) and high-quality epitaxy on silicon (3).

A large number of nonstoichiometric CeO_{2-x} phases with fluorite-related superstructures have been produced at high temperatures under oxygen-deficient conditions (4–9). For example, Ce_7O_{12} ($x = 0.29$) has a rhombohedral or hexagonal crystal symmetry (6), $Ce_{19}O_{34}$ ($x = 0.22$) triclinic (8), and Ce_6O_{11} ($x = 0.17$) monoclinic (*m*-) according to *in situ* X-ray diffraction study up to 855°C in vacuum and thermodynamic consideration (9). At higher temperatures, these ordered phases have a wide composition range according to combined X-ray, neutron and electron diffraction studies of the series Ce_nO_{2n-2} (8).

Recently, transmission electron microscopic (TEM) observations indicated that the cubic (*c*-) fluorite-type CeO_2 nanocrystals formed by laser ablation deposition in air are predominantly {111} octahedral (10), which tend to form coalescence twinning by impingement over {111} faces (11). These crystallites, when accumulated on surface oxidized Si(100) or soda-lime glass, have preferred orientation (111) due to deposition and coalescence of the crystallites with {111} as the contact plane (10). Such an artificial epitaxy depends on the shape of the crystallites in assembly (10), rather than surface relief of the substrate (12).

In this research, nonstoichiometric CeO_{2-x} coating was overlaid on transparent soda-lime glass substrate by laser ablation of CeO_2 target in vacuum in order to study optical property anisotropy as a result of nonstoichiometry of the CeO_{2-x} condensates under the influence of oxygen uptake from the silicate substrate. We also focused on artificial epitaxy of the coating in terms of rotation–coalescence of nanometer-size condensates and their organization into regular domains. These results shed light on oriented assembly of nanocrystals in general, and are of particular importance in understanding optical property anisotropy and preferred orientation of vapor-deposited CeO_{2-x} nanocrystals on a silica or silicate substrate that supplies oxygen in vacuum.

2. EXPERIMENTAL

Powders of CeO_2 (Cerac 99.9% pure) were dry pressed at 100 MPa into pellets and then sintered at 1600°C for 4 h followed by cooling in an open-air furnace. The target was subject to CO_2-laser (PRC, FH-3000, 10.6 μm in wavelength, beam mode: TEM00 + 01*) treatments at a specified power input (420 W) and time period (45–60 s) in vacuum (1.3 to 5×10^{-4} Pa) in order to form coating on the soda-lime glass. Copper slab (a good reflector with respect to laser beam) with a cylindrical hole, 16 mm in diameter and 10 mm in height, was used to hold the sintered pellet

[1]To whom correspondence should be addressed. FAX + 886-7-5254099. E-mail: pshen@mail.nsysu.edu.tw.

0022-4596/02 $35.00

which may become more or less spheroid during laser ablation (13). Preheating at a lower power input than the set value was required to avoid flipping of the pellet. A relatively high vacuum at 5×10^{-4} Pa and a target-to-substrate distance of about 120 mm gave the most adhered coating on the substrate according to the scratch test with a sharp needle. The samples fabricated under this condition were used for the present characterization of optical property anisotropy, crystal structures and lattice imperfections.

XRD (Cu$K\alpha$, 35 kV, 25 mA, step scanning from 20° to 100° at 0.05° increment with 2 s per step) was used to determine the preferred orientation of the as-deposited yellowish CeO_{2-x} coating and the crystal structures of the powders removed from the still yellowish, i.e., before being oxidized as whitish, coating. The diffraction peaks of the CeO_{2-x} were indexed according to *c*-fluorite cell, whereas those of minor Ce_6O_{11} phase as a primitive *m*-cell (9).

Optical microscopy under plane-polarized light was used to study optical property anisotropy, in particular, the pleochroism and birefringence of the CeO_{2-x} condensates that deposited as columnar domains on the glass substrate. The 2V angle as defined by the two optic axes, in terms of a refractive-index indicatrix, of the CeO_{2-x} crystal was measured from an interference figure under conoscopic observation.

Powdery material was retrieved predominantly from the yellowish coating and ultrasonically vibrated in isopropanol followed by sedimentation on copper grids overlaid with a carbon-coated collodion film for TEM observations using a JEOL 3010 instrument operating at 300 and 200 kV for imaging and energy dispersive X-ray (EDX) analysis, respectively.

3. RESULTS

The top coating prepared by laser ablation deposition in vacuum always appeared yellowish under naked eye, indicating the presence of Ce^{3+} as expected for nonstoichiometric CeO_{2-x}. The color, however, became whitish toward the edge of the coating where a thin bottom layer was exposed.

XRD of the powder retrieved predominantly from the yellowish part of the coating gave characteristic (043), (211) and (230) peaks of Ce_6O_{11} (indexed according to space group $P2_1/c$, JCPDS file 32-196) (9) in addition to others superimposed with *c*-fluorite-type peaks (Fig. 1). These extra peaks were of lower intensity than the fluorite peaks, indicating that a superlattice has been formed as the case of that characterized previously by XRD at high temperature (between 790°C and 855°C) and in vacuum (9). The 10 d-spacings of *c*-fluorite-type phase from Fig. 1 were used for least-squares refinement of the lattice parameters. It turned out to be 0.5426 ± 0.0003 nm, slightly larger than that of stoichiometric CeO_2 (JCPDS file 4-0593). This can be attributed to the substitution of larger cation Ce^{3+}

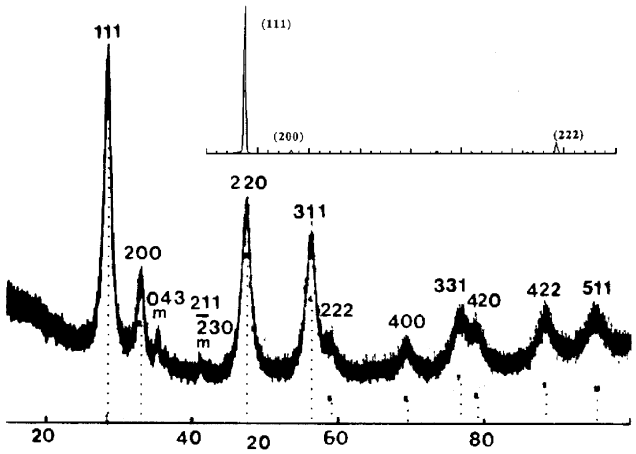

FIG. 1. XRD (Cu$K\alpha$) trace of powders retrieved from CeO_{2-x} coating deposited on soda-lime glass by laser ablation deposition in vacuum, showing characteristic Ce_6O_{11} peaks (denoted as *m*-phase and indexed here as a primitive *m*-cell (9) in addition to others superimposed with those of *c*-CeO_{2-x}. The inset shows XRD trace taken from the as-deposited yellowish coating with a strong (111) peak, its multiple (222), and barely visible (200) of *c*-fluorite phase, but the peaks of the Ce_6O_{11} phase are hardly seen due to the preferred orientation effect.

(0.1143 nm) for Ce^{4+} (0.097 nm) in coordination number of 8 (14) to form a nonstoichiometric *c*-CeO_{2-x} phase. The as-deposited yellowish coating has a preferred orientation (111) as indicated by XRD trace in the inset of Fig. 1 shows a strong (111) peak, its multiple (222), and barely visible (200) of *c*-fluorite phase. Due to the preferred orientation effect, the characteristic (043), (211) and (230) peaks of the Ce_6O_{11} phase were hardly observed.

Plan view of the whitish bottom coating showed columnar domains, which were finer in size toward the edge of the coating (Fig. 2). This optically isotropic bottom layer was

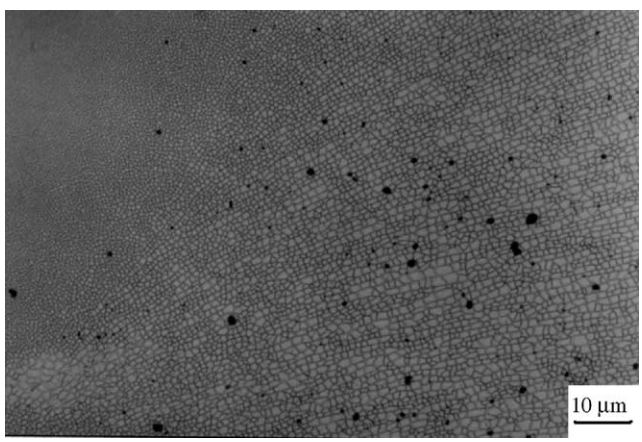

FIG. 2. Plan view of whitish bottom coating taken under optical polarized light (open polarizer), showing columnar domains progressively finer in size toward the edge of the coating.

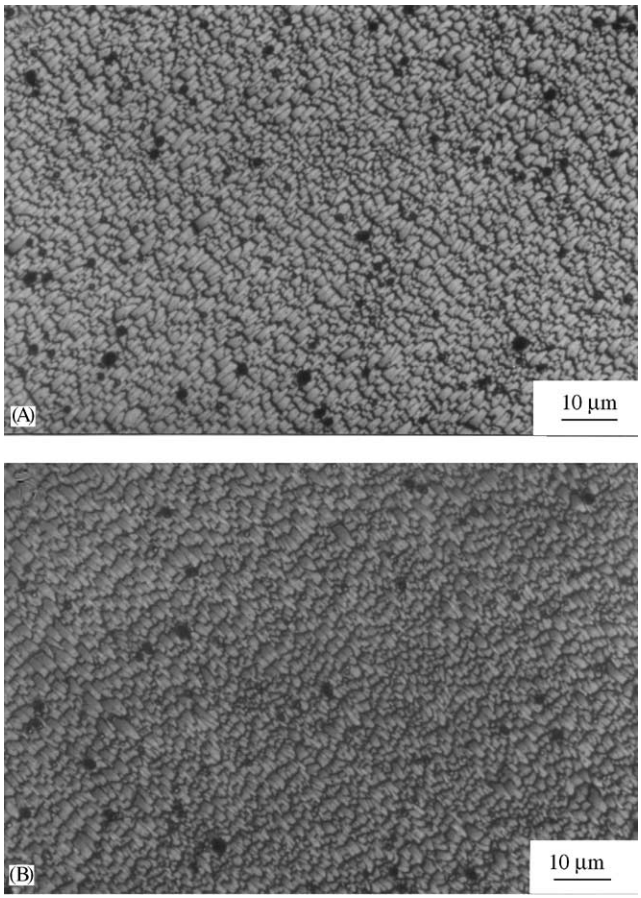

FIG. 3. Plan view of CeO_{2-x} top coating under crossed polarizers and gypsum accessory plate showing the CeO_{2-x} columns are length fast and nearly of the same crystal orientation: (A) and (B) are 45° clockwise and counterclockwise from the extinction position, respectively.

exposed from place to place to show complete extinction under crossed polarizers (Fig. 3). The columnar domains showed pale green to gray pleochroism (i.e., anisotropic optical absorption under open polarizer (15), and low birefringence (i.e., interference color under crossed polarizers) (Fig. 4). The lath-like columnar domains are in fact length fast with characteristic subtraction (yellow) and addition of (blue) interference color when aligned along NE–SW direction and NW–SE, respectively, under an accessory gypsum plate (Fig. 4).

Interference figure taken under conoscopic observation of columnar domains in parallel assembly showed a biaxial-positive indicatrix, which enabled the determination of a 2V angle of 40°. As discussed latter, Ce_6O_{11}-like units in equilibrium with CeO_2 or defect clusters of optically biaxial nature may account for such an optical property anisotropy.

TEM indicated that the agglomerated powdery materials removed from the coating consists of coalesced nanocrystals (Fig. 5), which gave a ring diffraction pattern of c-fluorite-like-type, yet (111) is much stronger with a preferred arc. A further magnified view from region A in Fig. 5 showed well-developed $\{111\}$ facets of CeO_{2-x} in exact [110] zone axis (Fig. 6A). The $\{111\}$ and (200) fringe separations are 0.31 and 0.27 nm, respectively, in agreement with XRD results of c-CeO_{2-x}. The columnar domain in region B was also magnified to show edge dislocation arrays, which were formed as a result of imperfect attachment over well-developed (111) planes and surface steps (Fig. 6B). The Ce_6O_{11} hardly survived the dispersion in isopropanol during TEM sample preparation, yet highly defective CeO_{2-x} nanoparticles with varied d-spacings were still observed (Fig. 6), which could be attributed to oxygen vacancies and defect clusters analogous to other fluorite-related intermediate rare-earth oxides (16).

EDX analysis of the coalesced nanocrystals showed no appreciable outward diffusion of cations from the substrate. Yet, outward diffusion of oxygen could possibly contribute to the formation of whitish CeO_2 interlayer with isotropic optical property.

4. DISCUSSION

4.1. CeO_2/CeO_{2-x} Phase Equilibrium and Defects

In contrast to nearly defect-free CeO_2 that condensed in air (10), the nonstoichiometric CeO_{2-x} condensed in vacuum showed varied (111) d-spacings, apparently due to varied extent of oxygen deficiency, and hence varied Ce^{3+}/Ce^{4+} ratio more or less with yellowish color. As mentioned, a number of nonstoichiometric CeO_{2-x} phases with fluorite-related superstructures have been produced at high temperatures under oxygen-deficient conditions (4–9). Among them, the monoclinic and the least oxygen deficient Ce_6O_{11} (8, 9) is in agreement with the observed optical properties and the phase equilibrium with stoichiometric CeO_2. This interpretation is supported by XRD of the as-deposited coatings and by our additional observations that the yellowish CeO_{2-x} converted into whitish CeO_2 upon exposure to air for days.

From the viewpoints of crystallography and defect chemistry, the optically anisotropic Ce_6O_{11} and CeO_{2-x} could be derived from the c-CeO_2 by disturbing its Ce (111) planes stacked in fcc-type sequence, such as Ce^{3+} in the substitution of smaller Ce^{4+} with charge-compensating oxygen vacancies and resultant-defect clusters. Such a superstructure formation in terms of cation and anion ordering in a host lattice was generally believed to be valid for fluorite-related compound (17). This effect may be important when the oxygen vacancy concentration is high in nanometer regime, as indicated by electrical conductivity measurements of cerium oxide thin films obtained by a polymeric precursor spin-coating technique (18). Still, condensation in the vacuum chamber and on the substrate should also affect the nucleation of CeO_{2-x}. Subsequent growth of the

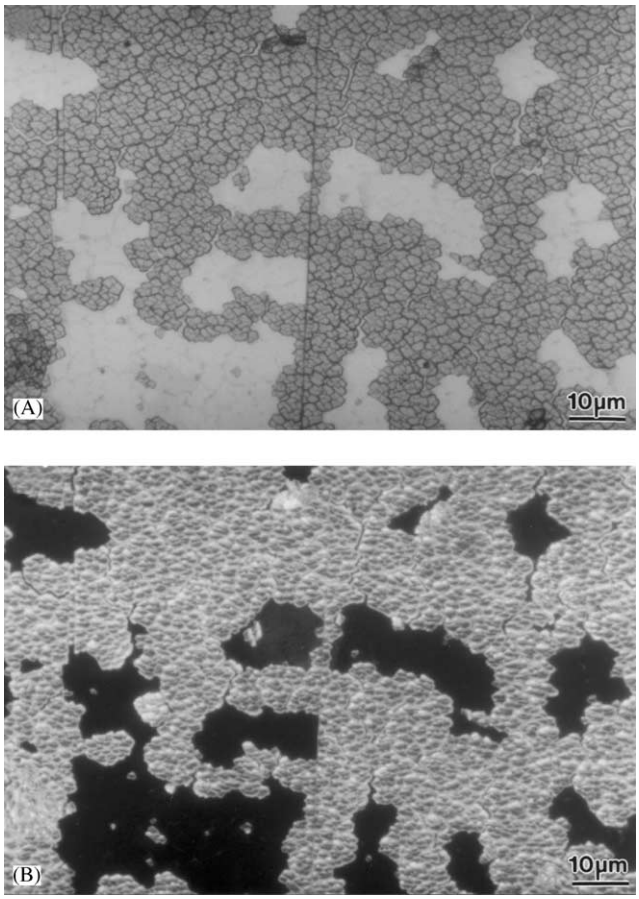

FIG. 4. Plan view of CeO_{2-x}/CeO_2 coating: (A) under open polarizer, (B) under crossed polarizers showing birefringent CeO_{2-x} top coating (bright) and isotropic CeO_2 (dark) bottom coating partly exposed.

condensates may be a combined result of ledge growth to form {111} surface steps and a coalescence event to form dislocations within columnar domains. Dislocations with (111) half-plane can be ascribed to coalescence of the crystallites over (111) contact plane, in accordance with well-developed {111} surfaces and steps of the crystallites in the columnar domains (Fig. 6). In this connection, dislocations (edge and/or screw type) were shown to generate from dislocation-free TiO_2 (anatase) nanoparticles when coalesced by the so-called imperfectly oriented attachment in hydrothermal solution (19).

4.2. *Artificial Epitaxy*

Preferred orientation of a crystalline deposit can be achieved regardless of the type of the substrate, as endeavored in the so-called artificial epitaxy (graphoepitaxy) on amorphous substrate with crystallographically arranged microrelief (12). Artificial epitaxy of the present CeO_{2-x} condensates also relies on the well-developed {111} surfaces of the condensates analogous to the case of deposition of octahedral CeO_2 condensates with {111}-preferred orientation on amorphous substrate (10).

Thermally activated rotation–coalescence of the crystallites over a substrate and within a film of considerable thickness may also cause preferred orientation of the assembled condensates. Experimentally, fcc metal crystallites have been proved to be able to migrate–rotate (20) and coalesce (21) on the free surface of single-crystal substrate regardless of the presence of surface steps (22) until low-energy epitaxial orientation with respect to the substrate was reached. (Refer to Ref. (23) for the retrospect of the experimental results and theoretical considerations of Brownian-type rotation of nonepitaxial crystallites on single-crystal substrate.) Einstein's molecular theory of heat, Eyring's transition state model and frictional force at a viscous interface were successfully adopted to formulate the diffusivity equation of the crystallite over the single-crystal substrate (24, 25). A critical temperature (T_c) must be reached for anchorage release and for the crystallites to move under a frictional force related to interfacial viscosity. In general, T_c is lower for a smaller particle size, and nanometer-size Au particles have been proved to migrate and coalesce on KCl(100) substrate at 94°C (20).

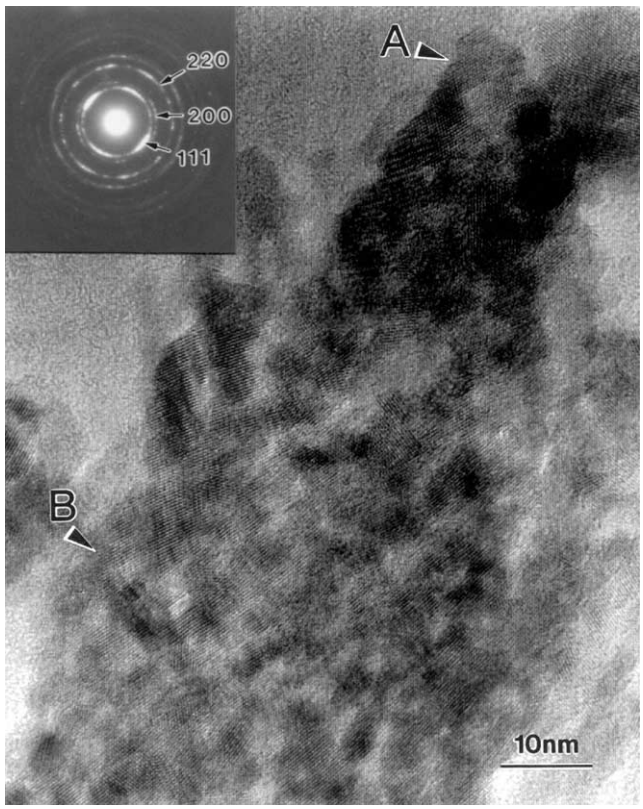

FIG. 5. TEM lattice image of powdery CeO_{2-x} agglomerates retrieved from the coating on glass. The inset shows selected area electron diffraction pattern (111)-preferred orientation of the assembled condensates.

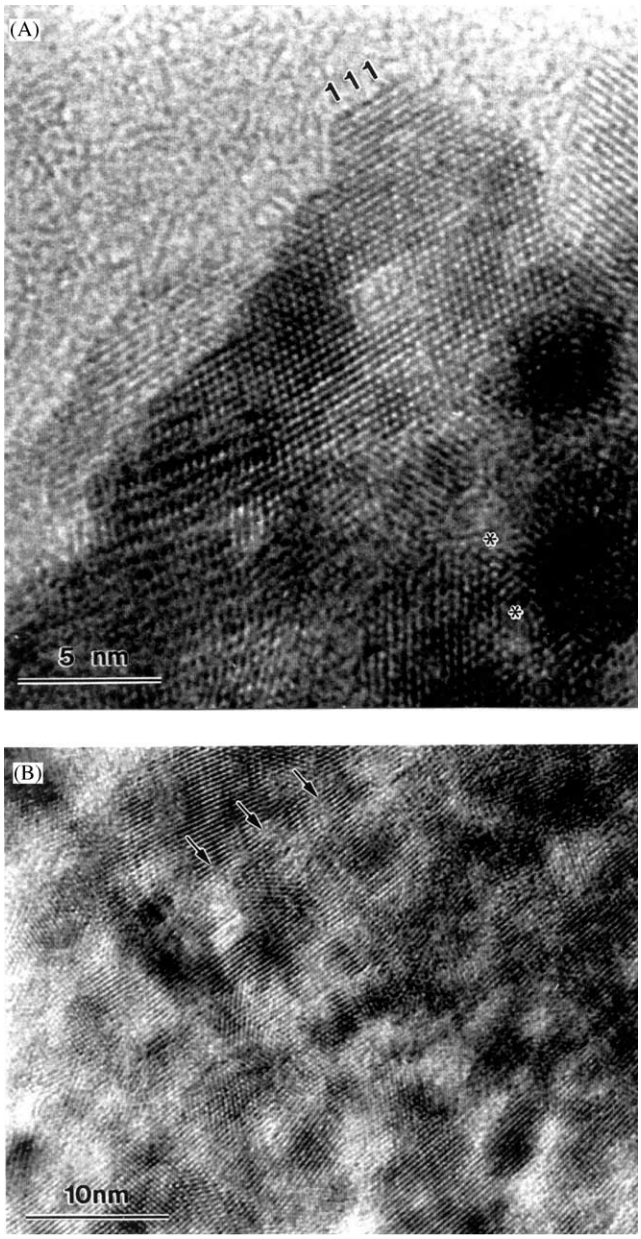

FIG. 6. Further magnified view from regions A and B in Fig. 5 showing respectively, well developed {111} facets of CeO_{2-x} in exact [110] zone axis and dislocation arrays (arrows) due to imperfect attachment of CeO_{2-x} nanocrystals over their well-developed (111) planes and steps. Note also highly defective CeO_{2-x} nanoparticles (denoted as *) due to oxygen vacancies and possible defect clusters.

Analogously, there is a size dependence of orientation change of intragranular particles in the bulk composites (26–28). In these experiments, the composites were prepared via a sintering route and subject to annealing above a critical temperature to activate rotation (26, 27) or rotation–coalescence (28) of the crystallites until epitaxy orientations with respect to host grain were reached. Given the nanometer size of the CeO_{2-x} condensates and heating effect of laser ablation deposition, the Brownian-type rotation–coalescence of the particles is expected to proceed not only over the substrate but also in the film of a considerable thickness. In this connection, the preferred orientation of TiC coating on steel substrate (29) and CeO_2 coating on Si or glass (10) was indeed found to change with deposition time.

Finally, it is noteworthy that atom clusters or molecules under the action of van der Waalls' interactions could assemble into a 3-D array. For example, CdSe (wurtzite-type structure) nanocrystals that slightly prolate along the *c*-axis were found to self-organize on quartz substrate as fcc quantum dot superlattice with the *c*-axis of the quantum dots parallel to each other (30). In accordance with their XRD and TEM results, the faceting and birefringence determined by optical microscopy under plane polarized light indicated ordering of the quantum dots into a 3-D array and the net alignment of their unique optical axes within the superlattice. Their arrangement was suggested to maximize van der Waalls' interactions between neighboring dots and with the substrate (30). It is also of interest to note that fcc array of C_{60} molecule transforms to simple cubic array below 249 K with accompanied orientation order of the C_{60} molecules (31). By contrast, the present CeO_{2-x} domains were not exactly of the same size and shape due to varied extent of growth and coalescence of the condensates, and thereby hardly self-assembled as 3-D array over glass substrate. Nevertheless, with (111)-preferred orientation of the columnar domains, the constituent Ce_6O_{11} or other fluorite-related defect clusters still have net alignment of their unique optical axes within the lattice to show birefringence.

5. SUMMARY

1. Laser ablation of CeO_2 target in vacuum produced Ce_6O_{11}/CeO_{2-x} composite coating on the soda-lime glass.
2. The top coating consists of optically anisotropic columnar domains conformable to monoclinic Ce_6O_{11} phase coexisting with cubic (*c*-) CeO_{2-x}, whereas the bottom coating is optically isotropic *c*-CeO_{2-x} due to oxygen uptake from the substrate.
3. The (111) preferred orientation of the coating can be rationalized by rotation–coalescence of nanometer size and {111}-faceted Ce_6O_{11}/CeO_{2-x} condensates on the amorphous substrate and/or within the coating.

ACKNOWLEDGMENTS

This research was supported by National Science Council under contract NSC88-2216-E-110-015. We thank Dr. L.Y. Kuo for early laser ablation runs with us.

REFERENCES

1. A. Tschöpe, J. M. Ying, and Y. M. Chiang, *Mater. Sci. Eng. A* **204,** 267 (1995).
2. H. Cordators, T. Bunluesin, J. Stubenrauch, J. M. Vohs, and R. J. Gorte, *J. Phys. Chem.* **100,** 785 (1996).
3. T. Nakazawa, T. Inoue, M. Satoh, and Y. Yamamoto, *Jpn. J. Appl. Phys.* **34,** 548 (1995).
4. D. J. M. Bevan, *J. Inorg. Nucl. Chem.* **1,** 49 (1955).
5. D. J. M Bevan and J. Kordis, *J. Inorg. Nucl. Chem.* **26,** 1509 (1963).
6. H. J. Rossell, *J. Solid State Chem.* **19,** 103 (1976).
7. H. T. Anderson and B. J. Wuensch, "Fast Ion Transport in Solids" (W. van Gool, Ed.). North-Holland, Amsterdam, 1973.
8. P. Knappe and L. Eyring, *J. Solid State Chem.* **58,** 312 (1985).
9. O.T. Sørensen, *J. Solid State Chem.* **18,** 217 (1976).
10. L. Y. Kuo and P. Shen, *Mater. Sci. Eng. A* **277,** 258 (2000).
11. W. H. Lee and P. Shen, *J. Cryst. Growth* **205,** 169 (1999).
12. E. I. Givargizov, "Oriented Crystallization on Amorphous Substrates," Plenum Press, New York, 1991.
13. Z. H. Chen, N. J. Ho, and P. Shen, *Mater. Sci. Eng. A* **196,** 253 (1995).
14. R. D. Shannon, *Acta Crystallogr. A* **32,** 751 (1976).
15. W. D. Nesse, "Introduction to Optical Mineralogy." Oxford University Press, New York, 1991.
16. P. Kunzmann and L. Eyring, *J. Solid State Chem.* **14,** 229 (1975).
17. H. J. Rossell, *J. Solid State Chem.* **27,** 115 (1979).
18. T. Suzuki, I. Kosacki, and H. U. Anderson, *J. Am. Ceram. Soc.* **84,** 2007 (2001).
19. R. L. Penn and J. F. Banfield, *Science* **281,** 969 (1998).
20. A. Masson, J. J. Métois, and R. Kern, *Surface Sci.* **27,** 463 (1971).
21. J. J. Métois, M. Gauch, A. Masson, and R. Kern, *Thin Solid Films* **11,** 205 (1972).
22. J. J. Métois, *Surf. Sci.* **36,** 269 (1973).
23. L. Y. Kuo and P. Shen, *Surf. Sci.* **373,** L350 (1997).
24. R. Kern, A. Masson, and J. J. Métois, *Surf. Sci.* **27,** 483 (1971).
25. J. J. Métois, M. Gauch, A. Masson, and R. Kern, *Surf. Sci.* **30,** 43 (1972).
26. J. Chen and P. Shen, *Scripta Mater.* **37,** 1287 (1997).
27. K. T. Lin and P. Shen, *Mater. Sci. Eng. A* **270,** 125 (1999).
28. S. R. Wang and P. Shen, *Mater. Sci. Eng. A* **251,** 106 (1998).
29. L. Y. Kuo and P. Shen, *Mater. Sci. Eng. A* **276,** 99 (2000).
30. C. B. Murray, C. R. Kagan, and M. G. Bawendi, *Science* **270,** 1335 (1995).
31. P. A. Heiney, J. E. Fischer, A. R. McGhie, W. J. Romanow, A. M. Denenstein, J. P. McCauley, and A. B. Smith, *Phys. Rev. Lett.* **66,** 2911 (1991).